A New FAPAR Analytical Model Based on the Law of Energy Conservation: A Case Study in China

Wenjie Fan, *Member, IEEE,* Yuan Liu, Xiru Xu, *Member, IEEE,* Gaoxing Chen, and Beitong Zhang

***Abstract*—The fraction of absorbed photosynthetically active radiation (FAPAR) characterizes the energy-absorption ability of the vegetation canopy. It is a critical input to many land-surface models such as crop growth models, net primary productivity models, and climate models. There is a great need for FAPAR products derived from remote-sensing data. The objective of this research is to develop a new instantaneous quantitative FAPAR model based on the law of energy conservation and the concept of recollision probability (p). Using the ray-tracing method, the FAPAR-P model separates direct energy absorption by the canopy from energy absorption caused by multiple scattering between the soil and the canopy. Direct sunlight and diffuse skylight are also considered. This model has a clear physical meaning and can be applied to continuous and discrete vegetation. The model was validated by Monte Carlo (MC) simulation and field measurements in the Heihe River basin, China, which proved its reliability for FAPAR calculations.**

***Index Terms*—Clumping index, FAPAR-P model, fraction of absorbed photosynthetically active radiation (FAPAR), recollision probability (p).**

I. Introduction

THE fraction of absorbed photosynthetically active radiation (FAPAR) is a critical eco-physiological variable for estimating canopy gross primary production (GPP) and is, therefore, the key variable influencing photosynthesis, transpiration, and energy balance in most soil-vegetation-atmosphere transfer (SVAT) models from leaf to landscape scale [1]–[12]. Many bio-physical FAPAR models have been developed to describe the interaction between biosphere and atmosphere, including multilayer models [13], discrete 2D and 3D models [14]–[16], simple single-layer big-leaf models [17]–[19], and sun-shade models [20]–[24] in ecological studies. These models and several of these surface schemes have been incorporated into regional or global climate models [17], [25]–[30]. Therefore, there is a great need for FAPAR products to provide input data. In addition, some experts have focused on the study of chlorophyll FAPAR [31].

Manuscript received October 15, 2013; revised January 29, 2014; accepted May 04, 2014. Date of publication June 17, 2014; date of current version November 04, 2014. This research has been supported in part by the National Basic Research Program of China under Grant 2013CB733402, in part by the National Natural Science Foundation of China under Grant 41271346, Grant 41230747, and Grant 91025006, in part by the National High Technology Research and Development Program of China under Grant 2012AA12A304, and in part by the National Supporting Technology Project under Grant 2012BAH29B03.

The authors are with the Institute of Remote Sensing and Geographical Information System, Peking University, Beijing 100871, China (e-mail: fanwj@pku.edu.cn; 2008.liuyuan.2008@163.com; xrxurs@126.com; gaoxingchen@gmail.com; noelzhang@pku.edu.cn).

Color versions of one or more of the figures in this paper are available online at http://ieeexplore.ieee.org.

Digital Object Identifier 10.1109/JSTARS.2014.2325673

Remote sensing can provide spatial distribution functions of land-surface properties including land cover, vegetation type parameters, vegetation structure, and light-use efficiency [32], [33]. Regional and global FAPAR products are now derived from multiple sensors, such as moderate-resolution imaging spectroradiometer (MODIS) [10], Sea-Viewing Wide Field-of-View Sensor (SeaWiFS) [12], and the Medium Resolution Imaging Spectrometer (MERIS) [34]. FAPAR products are often derived by two kinds of algorithms using remote-sensing data as constraints. The empirical methods have always been developed using satellite sensor-derived spectral vegetation indices [e.g., normalized difference vegetation index (NDVI) [8], [35]) or leaf area index (LAI [9]). However, the empirical parameters for these statistical methods are limited to a regional area at a certain period and are, therefore, hard to apply to new unknown larger areas over long time scales. To avoid the disadvantages of statistical methods, physical inversion methods have been proposed based on radiative transfer (RT) models [10], [12], [36]–[38]. The Joint Research Centre (JRC) FAPAR algorithm has been developed for MERIS and SeaWiFS [39]–[41] using measurements in the blue, red, and near-infrared spectral domains. The algorithm was based on the continuous vegetation canopy model [42] and the 6S model. Knyazikhin *et al.* [36] proposed a synergistic algorithm for calculating LAI and FAPAR based on the RT model. The RT model is separated into a black-soil problem and a scattering problem, each of which expresses canopy transmittance, reflectance, and absorbance based on the law of energy conservation. The MODIS LAI/FAPAR product is based on this algorithm. The two algorithms have a clear physical mechanism and are used to produce global products.

This research has discovered a new way to provide a simple analytical and reliable algorithm for FAPAR retrieval using remote-sensing data, which can be appropriate for various canopy structures and different levels of ambient radiation. Based on energy conservation and the concept of recollision probability, a new FAPAR-P model (FAPAR model based on p) has been developed which considers the effects of canopy structures, ambient radiation, and multiple scattering between soil and vegetation. The model has been validated by Monte Carlo (MC) simulation and *in-situ* simultaneous measurements, and a case study in China has been presented, which will be beneficial for understanding the physical mechanism of FAPAR retrieval.

II. Theory and Methodology

A. FAPAR Model for Continuous Vegetation

FAPAR is the fraction of incoming solar radiation that is absorbed by green vegetation in the spectral range from 400 to

700 nm. Assuming constant soil reflectance, FAPAR includes the direct absorption of radiation by the canopy $a_1(\lambda)$; and the part that is reflected by the background and then absorbed by the vegetation $a_2(\lambda)$. Therefore, the total energy fraction absorbed by the green canopy is

$$a(\lambda) = a_1(\lambda) + a_2(\lambda) \tag{1}$$

where λ is the wavelength. $a_1(\lambda)$ can be calculated if the background reflectance r_g is assumed to be zero. Then, the instantaneous FAPAR can be expressed by

$$FAPAR = \int_{0.4-0.7\ \mu\mathrm{m}} a(\lambda)d\lambda. \tag{2}$$

1) Fraction of Solar Radiation Directly Absorbed by the Canopy: Along the incident solar beam, the photons will be scattered (reflected or transmitted) or absorbed when they collide with the vegetation canopy. The probability of scattering is ω_l (ω_l is the single-scattering albedo), and the probability of absorption is $1-\omega_l$. The scattered photons can either directly penetrate the canopy boundary or collide again within the canopy. p_i represents the recollision probability at the ith collision time. A photon in the vegetation canopy can undergo several collisions until it penetrates the canopy or its energy becomes less than a threshold value. This can be regarded as the life cycle of a photon. Assuming that the soil is black, the total probability of scattering and absorption can be represented as $S_{bs}(\lambda)$ and $a_1(\lambda)$, respectively. The precondition of collision is that photons are intercepted by vegetation, so $S_{bs}(\lambda)$ and $a_1(\lambda)$ are conditional probabilities. Assume the probability that photons are intercepted by the canopy is i_0; because leaves are homogeneously distributed in the canopy, $i_0 = 1 - \exp(-\frac{G_i}{\mu_i}LAI)$. Therefore

$$S_{bs}(\lambda) + a_1(\lambda) = i_0 \tag{3}$$

where $\mu_i = \cos\theta_i$, θ_i is the solar zenith angle, G_i is the projection of leaves per unit ground area on the plane perpendicular to the incident solar beam, and LAI is the vegetation leaf-area index. The total probability of scattering is the sum of the scattering probabilities of each collision

$$S_{bs} = i_0(\omega_l(1-p_1) + \omega_l p_1 \omega_l(1-p_2) + \cdots). \tag{4}$$

If $p_1 = p_2 = p_3 = \cdots = p$, then $S_{bs} = i_0 \cdot \omega_l \cdot \frac{1-p}{1-\omega_l p}$, and, therefore, $a_1(\lambda)$ can be written as

$$a_1(\lambda) = i_0 - S_{bs} = i_0 \cdot \frac{1-\omega_l}{1-\omega_l p}. \tag{5}$$

Suppose that the downward radiance of diffuse skylight is approximately isotropic in hemispherical space. The average probability that diffuse skylight is intercepted by the canopy can be expressed as $\tilde{i}_0$. The irradiance of diffuse skylight reaching the canopy can be written as [43]

$$e = \int_{2\pi} L_a^{\downarrow} \cos\theta_i \cdot \left(1 - e^{-\frac{G}{\cos\theta_i}LAI}\right) d\Omega \tag{6}$$

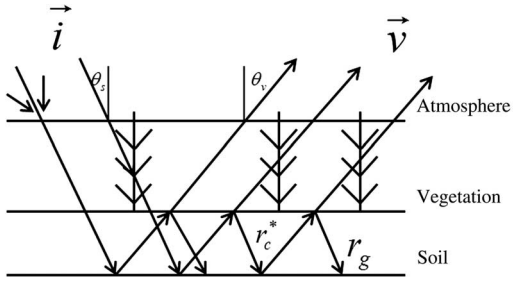

Fig. 1. Multiple interactions of photons with canopy and soil background.

where $L_a^{\downarrow}$ is the downward radiance and is approximately isotropic in 2π space, $d\Omega$ is the differential solid angle, $d\Omega = \sin\theta_i d\theta_i d\phi_i$, and ϕ_i is the incident azimuth.

For the continuous vegetation canopy, the relationship between irradiance of diffuse skylight and LAI can be obtained by numerical integration when leaf-angle distribution is spherical

$$e = \left(1 - e^{-0.8LAI^{0.9}}\right) \cdot E \tag{7}$$

where $E = \pi \cdot L_a^{\downarrow}$ (when $G = 0.5$).

The average probability that diffuse skylight is intercepted by the canopy in 2π space can be expressed as $\tilde{i}_0$. When the vegetation type is spherical, $\tilde{i}_0$ can be expressed as

$$\tilde{i}_0 = 1 - \exp\left(-0.8LAI^{0.9}\right). \tag{8}$$

When the leaf-angle distribution function is nonspherical, the constant parameters -0.8 and 0.9 should be adjusted, but the form of the empirical equation remains unchanged.

The diffuse skylight proportion of total incident radiation can be expressed as $\beta = E/(E + \mu_i F)$, where E is the irradiance of diffuse skylight and $\mu_i F$ is the direct solar irradiance for the horizontal plane. Considering the contributions of both direct and diffuse solar radiation, $a_1(\lambda)$ is the weighted sum of the two parts

$$a_1(\lambda) = i_0 \cdot \frac{1-\omega_l(\lambda)}{1-p\omega_l(\lambda)} \cdot (1-\beta) + \tilde{i}_0 \cdot \frac{1-\omega_l(\lambda)}{1-p\omega_l(\lambda)} \cdot \beta. \tag{9}$$

2) Absorption Caused by Vegetation-Soil Multiple Scattering: In fact, the black-soil assumption adopted above is an ideal condition. If soil reflectance is considered, FAPAR should include the part that is reflected by the background and then absorbed by vegetation.

Two energy components will reach the soil surface through the canopy: 1) the proportion of the incident radiation that directly reaches the soil without interacting with the canopy (f_1) and 2) the proportion that reaches the soil after one or more scattering events within the canopy (f_2), as shown in Fig. 1.

Suppose that $G_{i,v} = 0.5$, $r_l(\lambda) \cong \tau_l(\lambda)$, $r_l(\lambda)$ is leaf reflectance, $\tau_l(\lambda)$ is leaf transmittance, and the diffuse radiation that reaches the bottom interface of the canopy is approximately isotropic in the half-space; then the average interception probability is $\tilde{i}_0$.

The first part depends on the canopy transmittance along the incident direction of light, which can be expressed as

$$f_1 = (1-i_0) \cdot (1-\beta) + (1-\tilde{i}_0) \cdot \beta. \tag{10}$$

The first part of the right side of (10) represents the contribution of direct sunlight, and the second part represents the contribution of diffuse skylight.

For simplicity, let us assume that leaf reflectance $r_l(\lambda)$ is equal to leaf transmittance $\tau_l(\lambda)$, $r_l \cong \tau_l$, and that scattering within the canopy can be considered isotropic. Then the proportion that reaches the soil after one or more scattering events within the canopy can be expressed as

$$f_2 = i_0 \cdot \frac{\omega_l(1-p)}{1-\omega_l p} \cdot \frac{1}{2} \cdot (1-\beta) + \tilde{i}_0 \cdot \frac{\omega_l(1-p)}{1-\omega_l p} \cdot \frac{1}{2} \cdot \beta. \quad (11)$$

This means that f_2 is the sum of two parts, the contribution of sunlight reaching the ground after interception by the vegetation canopy through scattering, and the contribution of diffuse skylight reaching the ground after interception by the canopy through scattering.

Therefore, the absorption caused by canopy-soil multiple scattering can be expressed as

$$a_2(\lambda) = (f_1 + f_2) \cdot \frac{r_g}{1 - r_g r_c^* \tilde{i}_0} \cdot \tilde{i}_0 \cdot \frac{1-\omega_l}{1-p\omega_l} \quad (12)$$

where r_c^* is the diffuse reflectance of the vegetation canopy (Fig. 1) $r_c^* = \frac{1}{2} \cdot \frac{\omega_l(1-p)}{1-\omega_l p}$.

Therefore, FAPAR can be obtained as an integral of bands ranging from 400 to 700 nm using (2) when $a_1(\lambda)$ and $a_2(\lambda)$ are known.

B. FAPAR Model for Noncontinuous Vegetation

In nature, leaves (the main scattering elements) are clustered on different scales within the crown and from one crown to another. Therefore, different vegetation types can be considered in some way as superimposed clusters on different scales, meaning that continuous homogeneous vegetation is only an assumption under ideal conditions. Because of the existence of clusters, leaves shade each other, and, therefore, canopy transmittance increases in some directions [44].

The negative exponential form of transmittance ($P(\theta) = \exp(-\frac{G_i}{\mu_i} \cdot LAI)$) is the solution of the differential term in the RT equation under the assumption that there is no mutual shading among leaves. Nilson [44] first introduced a parameter Ω_i (called the clumping index or Nilson index $0 \le \Omega_i \le 1$) to describe the clumping effect among leaves. In addition, the concept of effective leaf-area index (LAI_e), was proposed to replace the original LAI by multiplying by the clumping index (W_i), i.e., $LAI_e = W_i LAI_a$. With the introduction of the clumping index and LAI_e, the transmittance formula can be widely used for various types of vegetation canopies [45], [46].

The absorption and scattering probabilities of photons are determined by $1-\omega_l$ and ω_l, respectively, when photons collide with leaves, whereas they are not associated with other factors (such as whether the leaves are illuminated by the Sun). The number of collisions in a photon's life cycle depends only on the recollision probability, p [36], [47]. p is a function of LAI, and, therefore, the form of the total absorption probability equation remains the same for different vegetation types, the only difference being the use of LAI_e instead of LAI.

The FAPAR model for noncontinuous vegetation should, therefore, be corrected to

$$a_1(\lambda) = i_0(\Omega) \cdot \frac{1-\omega_l(\lambda)}{1-p(\Omega)\omega_l(\lambda)} \cdot (1-\beta) + \tilde{i}_0(\Omega) \cdot \frac{1-\omega_l(\lambda)}{1-p(\Omega)\omega_l(\lambda)} \cdot \beta \quad (13)$$

$$a_2(\lambda) = (f_1(\Omega) + f_2(\Omega)) \cdot \frac{r_g}{1 - r_g r_c^* \tilde{i}_0(\Omega)} \cdot \tilde{i}_0(\Omega) \cdot \frac{1-\omega_l(\lambda)}{1-p(\Omega)\omega_l(\lambda)}. \quad (14)$$

III. Results and Analysis

A. Comparison With MC Simulation

MC simulation is a stochastic simulation calculation method based on the RT model [48]–[50]. The results can be obtained through repeated random sampling, and the RT process for photons in the canopy can be simulated according to different canopy structures. Many studies of canopy reflectance have been conducted using MC simulation. Govaerts *et al.* [50] described four steps that are used to calculate the RT process within the canopy: generating the rays (photons) and determining the parameters of the photons that collide with objects (scenes), the type of collision and scattering direction, and the information on the ray path (counting). FAPAR is a ratio. The absorption and scattering probabilities of photons depend on ω_l only in the collision process, but are not affected by whether leaves are illuminated by the Sun. As proved in Section II-A2, the interception probability equation is the same for any vegetation type as long as the effective leaf-area index is used to conduct the MC simulation instead of the leaf-area index. This means that the MC method can undoubtedly be used to simulate canopy FAPAR. A random flowchart of photon-transfer processes in the canopy has been used [51].

The parameters used include:

Photon incident zenith angle θ_s: $0-90°$;

Photon incident azimuth ϕ_s: $0-180°$;

Leaf-angle distribution type: level, straight, tilted, extreme, uniform, and spherical (select one);

Leaf-area index of canopy: 0–10;

Termination threshold of photon energy: 0.001;

Photon number: if the value is greater than 10^6, 10^6 is used.

The leaf reflectance, leaf transmittance, and soil reflectance values used in the simulation were obtained from the Leaf Optical Properties Experiment 93 (LOPEX93) database. According to the spectral characteristics of soil and vegetation, 18 points were nonuniformly sampled in the $0.4-0.7$ μm region. The resulting spectra are shown in Fig. 2.

1) Empirical Expressions for p and $\tilde{i}_0$ Compared With MC Simulation: For a continuous canopy, Smolander and Stenberg [52] have proposed an empirical relationship between the recollision probability (p) and LAI when leaf-angle distribution is spherical ($G = 0.5$). In fact, the recollision probability has

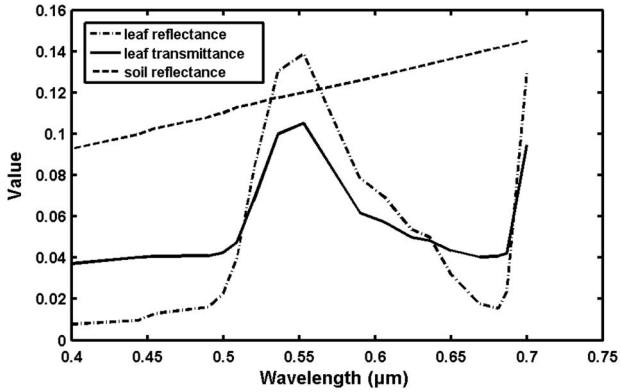

Fig. 2. Soil reflectance, leaf reflectance, and transmittance spectra in the $0.4-0.7$ μm region.

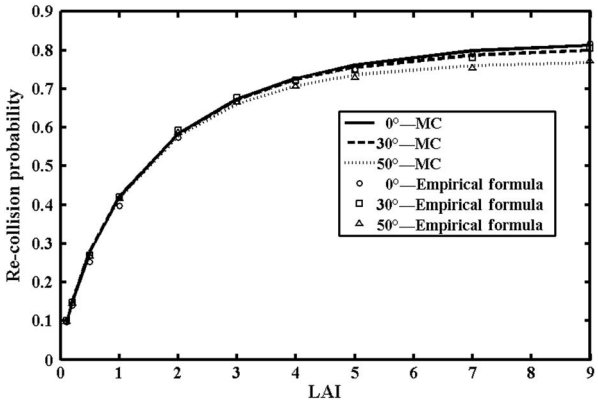

Fig. 3. Comparison of recollision probability between empirical formula and MC.

been found to vary with solar zenith angle, and, therefore, the empirical formulas should be amended to read

$$p = 0.7 \cdot \exp(0.0155 \cdot LAI) - 0.66 \cdot \exp(-0.71 \cdot LAI) \tag{15}$$

$$p = 0.71 \cdot \exp(0.014 \cdot LAI) - 0.66 \cdot \exp(-0.78 \cdot LAI) \tag{16}$$

$$p = 0.7 \cdot \exp(0.01 \cdot LAI) - 0.66 \cdot \exp(-0.8 \cdot LAI). \tag{17}$$

Note that (15)–(17) are the empirical expression when $\mathrm{G} = 0.5$ and solar zenith angle is 0°, 30°, and 50°, respectively. The empirical relationship can also be obtained at other solar zenith angles.

To evaluate the empirical relationship, p was calculated using MC simulation at a given incident solar zenith angle. The relationship between p and LAI_e from MC coincided well with the results of the empirical formula (Fig. 3).

Meanwhile, to verify the empirical equation for the average interception probability $\tilde{i}_0$, the number of photons which were intercepted by the vegetation canopy was counted in hemispherical space. The comparison is shown in Fig. 4. It is apparent that the difference is negligible between the two independent methods. It has also been proved that the empirical equation for $\tilde{i}_0$ is reliable.

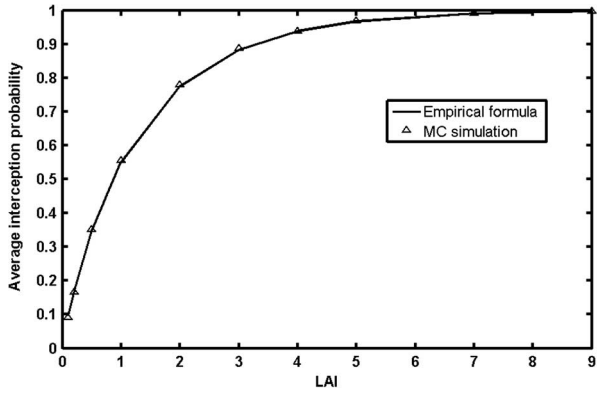

Fig. 4. Comparison of average recollision probability between empirical formula and MC.

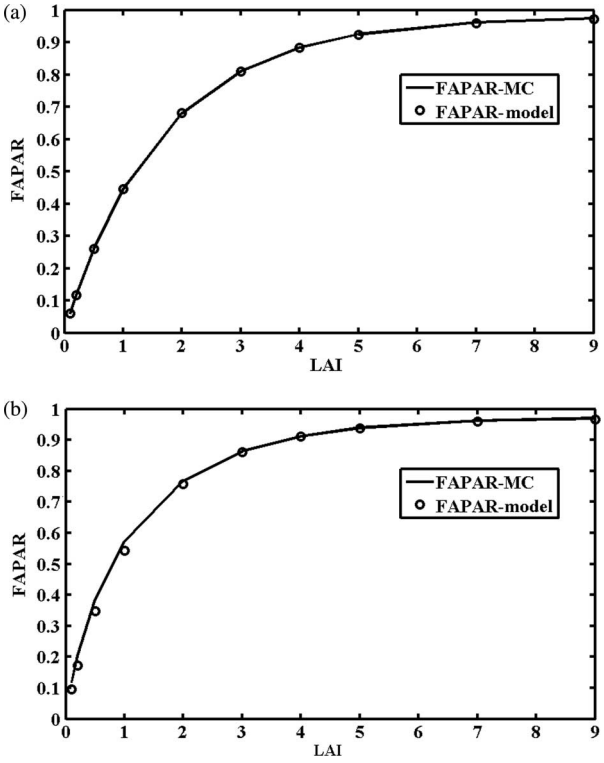

Fig. 5. Relationships between FAPAR and LAI_e in MC and the model. (a) FAPAR ($\theta = 30°$, $\beta = 0$). (b) FAPAR ($\beta = 1$).

2) MC Simulation for Continuous Vegetation: The continuous-vegetation FAPAR was simulated by MC, and the results were compared with those obtained by the FAPAR model under different situations. When the leaf angular distribution type is spherical ($\mathrm{G} = 0.5$), the FAPAR values for different LAI_e were simulated using the MC method, with the results shown in Fig. 5. It is clear that the difference between the MC simulation and the model is negligible.

When the incident solar zenith angle is 30° and $\beta = 0$ [Fig. 5(a)], the difference (less than 0.32%) between the model outputs and MC simulations is negligible. Fig. 5(b) shows that when $\beta = 1$, differences do exist between the two values, but they decrease with increasing LAI. The errors are less than 0.42% when LAI is greater than 3. When LAI is small, there are few

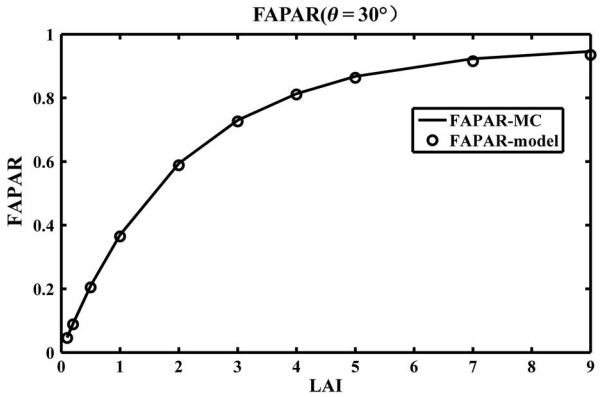

Fig. 6. Relationships between FAPAR and LAI_e in MC and the model for row crops.

leaves, and the interception of diffuse radiation is limited, leading to fluctuation of the FAPAR model and the MC simulations.

3) FAPAR Model for Row Crops: The FAPAR model for row crops was also evaluated by MC simulation. Fig. 6 indicates that the difference between MC and the model is small (less than 0.3%) when the ridge width $l_1 = 0.2$ m, the between-ridge width $l_2 = 0.3$ m, G $= 0.5$, and $\phi = 90°$. The model calculated the clumping index of row crops according to Yan's method [53]. Model bias increases with LAI, but the largest bias is limited to less than 1% when LAI is greater than 7. These results indicate that the model can be reliably applied to row crops.

B. Analysis of Parameters in the FAPAR Model

Many factors affect FAPAR retrieval and must be analyzed to provide theoretical support for it. Therefore, leaf-area index, solar zenith angle, soil reflectance, and the proportion of diffuse skylight were chosen and analyzed because of their relatively high importance.

Due to the discontinuity of the spectral bands for most remote sensors, 18 wavelengths within the $0.4-0.7$ μm spectral range were nonuniformly sampled to mimic this discontinuity effect. Leaf reflectance and transmittance as well as soil reflectance at the chosen 18 wavelengths were obtained from the LOPEX93 database. The canopy FAPAR was calculated as the integral of the 18 FAPAR values according to solar radiation at each wavelength.

1) Effect of Solar Zenith: When the vegetation type is spherical and $\beta = 0$, the relationship between FAPAR and solar zenith is shown in Fig. 7. Fig. 7 shows that FAPAR increases with solar zenith angle when LAI is fixed, but that the rate of increase gradually diminishes, which can be physically explained by the elongation of the photon travel path inside the canopy and the increased probability of collisions between photons and leaves.

When $\beta = 0.9$ [Fig. 7(b)], the effect of solar zenith angle becomes weaker because diffuse skylight is the main form of incoming solar radiation and is isotropic.

2) Effect of Single-Scattering Albedo: Because single-scattering albedo $\omega(\lambda)$ is the sum of leaf reflectance $r_l(\lambda)$ and leaf transmittance $\tau_l(\lambda)$, $\omega(\lambda) = r_l(\lambda) + \tau_l(\lambda)$, and $r_l(\lambda) \cong \tau_l(\lambda)$ (assumed). Therefore, three kinds of leaf reflectance (Rabbitbrush, Lawn Grass, and Juniper Bush, from the USGS Spectral Library)

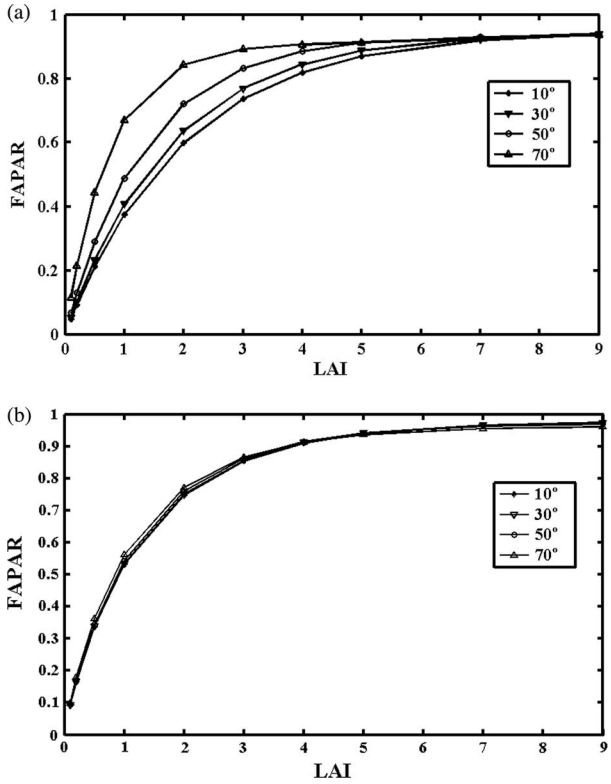

Fig. 7. Simulated relationships between FAPAR and solar zenith angle from the model under different β. (a) FAPAR ($\beta = 0$). (b) FAPAR ($\beta = 0.9$).

were selected to analyze the effect of single-scattering albedo in the FAPAR model.

Similarly, 18 points of leaf reflectance (corresponding to the wavelengths mentioned earlier) were nonuniformly sampled in the $0.4-0.7$ μm spectral range; the soil reflectance can be used with the same points as above (Fig. 2).

The relationships between canopy absorption and single-scattering albedo are shown in Fig. 8 under the same LAI and β. The main reflection band is the green (0.55 μm) band, whereas the main absorption bands of leaves are the red (0.65 μm) and blue (0.45 μm) bands; therefore, canopy absorption changes with changes in wavelength. The leaves exhibit high reflectance in the near-infrared band, meaning that canopy absorption begins to decline at approximately 0.7 μm. In the $0.4-0.7$ μm range, the general trend in canopy absorption moves from descending to ascending and then to descending again. In addition, canopy absorption varies with differences in single-scattering albedo. The greater the single-scattering albedo, the smaller is the canopy absorption.

3) Effect of Soil Reflectance: To discuss and analyze the impact of different soil types on modeled FAPAR, three kinds of soil with large differences in reflectance were selected: grayish-brown loam, gray silty clay, and reddish-brown fine sandy loam (Fig. 9). The 18 soil-reflectance points (corresponding to those mentioned earlier) were nonuniformly sampled in the $0.4-0.7$ μm spectral range from the Johns Hopkins University (JHU) database.

Fig. 10 shows the contribution of background reflectance to modeled FAPAR. It is clear that higher soil reflectance produces a larger FAPAR value for the canopy. The results also

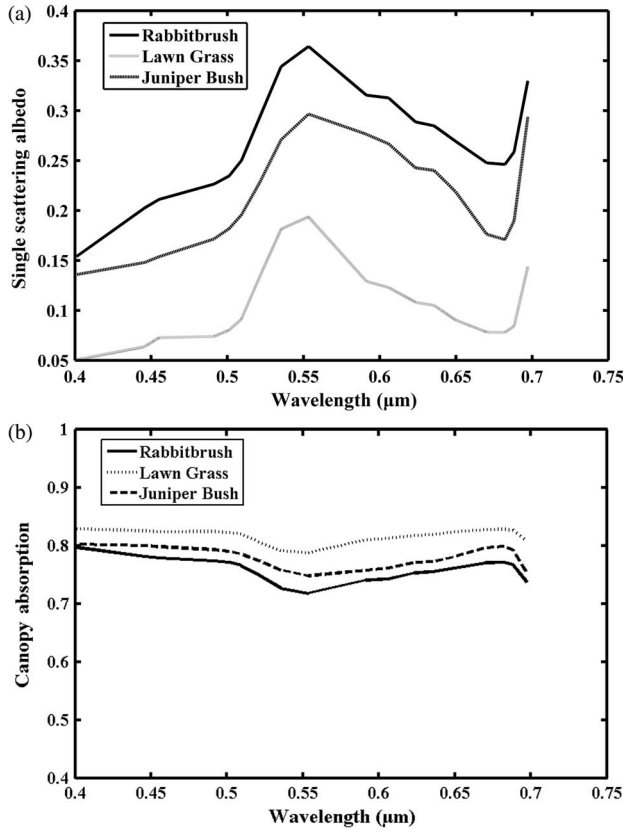

Fig. 8. Relationships between canopy absorption and single-scattering albedo from the model: (a) spectra of single-scattering albedo and (b) canopy absorption under different $\omega(\lambda)$.

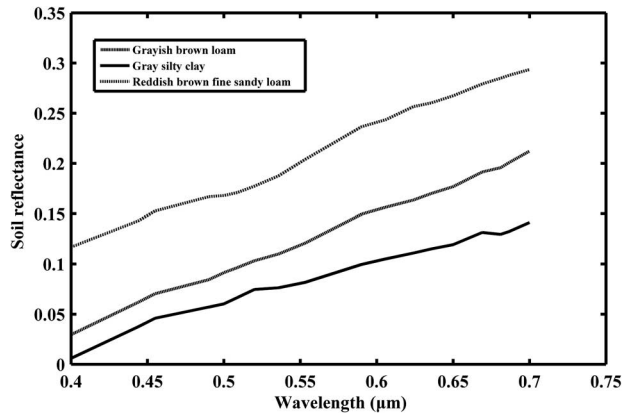

Fig. 9. Reflectance spectra of the three kinds of soil in the $0.4-0.7$ μm spectral range.

imply that canopy absorption along the outgoing path cannot be neglected. FAPAR changes only slightly as β changes from 0 to 0.5.

4) Effect of Diffuse Skylight Proportion (β): Fig. 11 shows the relationship between FAPAR and β. It shows that the contribution of diffuse skylight to canopy FAPAR cannot be ignored. FAPAR increases with increasing β value when LAI is fixed. When θ is large ($\theta = 60°$), the relationship between FAPAR and β is weakened, so the FAPAR is less dependent on beta when θ is increased to 60°, as shown in Fig. 11(b).

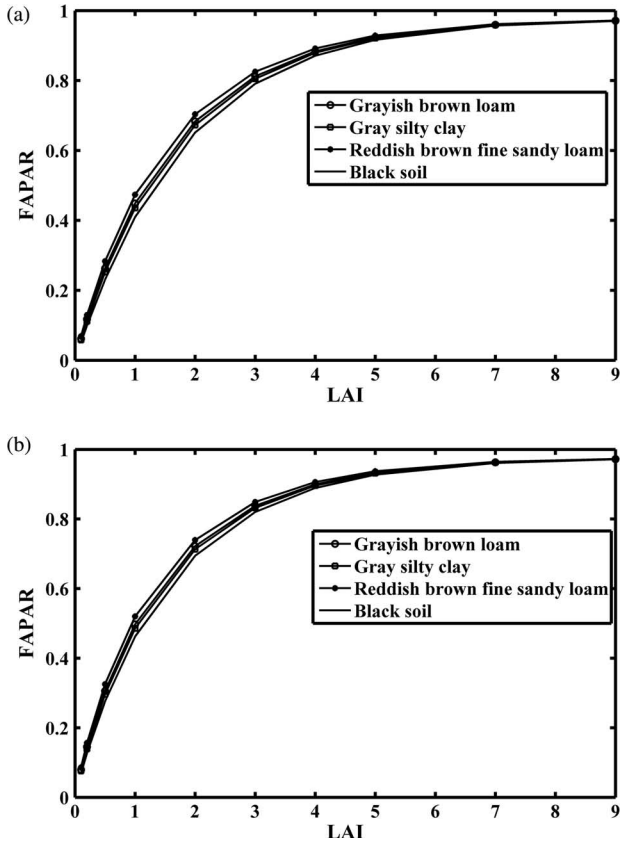

Fig. 10. Relationships between FAPAR and soil reflectance from the model under different β. (a) FAPAR ($\beta = 0, \theta = 30°$). (b) FAPAR ($\beta = 0.5, \theta = 30°$).

IV. Field Validation

A. Study Region and Data

1) Study Region: The Yingke oasis station, which is located in Zhangye City at the midstream point of the Heihe Basin, was selected as the study area and is shown in Fig. 12. Yingke oasis station is covered by a large area of crops in summer, including corn, wheat, barley, and flax. The landscape classification and vegetation distribution for the study area are available at http://heihe.westgis.ac.cn/.

2) Field Measurement: By measuring the incoming solar flux $I^{\downarrow}_{\mathrm{TOC}}$, flux to the ground $I^{\downarrow}_{\mathrm{Ground}}$, flux from the ground $I^{\uparrow}_{\mathrm{Ground}}$, and outgoing solar flux $I^{\uparrow}_{\mathrm{TOC}}$ [12], FAPAR was calculated by using (18):

$$FAPAR = \left(I^{\downarrow}_{\mathrm{TOC}} - I^{\downarrow}_{\mathrm{Ground}} + I^{\uparrow}_{\mathrm{Ground}} - I^{\uparrow}_{\mathrm{TOC}}\right)/I^{\downarrow}_{\mathrm{TOC}}. \quad (18)$$

The four items were measured using a SunScan v1.01 probe at 15-min intervals between 13:00 and 18:00 every day from July 4, 2012 to July 8, 2012. Measurements were conducted at $38°51'13.8''$N, $100°22'17''$E. The corn was in its growing season, and the ridges were covered by leaves, as shown in Fig. 13. 249 sets of data were gathered from July 4 to 8 using SunScan and included sets for FAPAR daily change and sets for various quadrats randomly distributed in the study area.

3) Data Processing: An image obtained from the HJ-1B satellite at 03:52:46 GMT, July 8, 2012, with a spatial resolution of

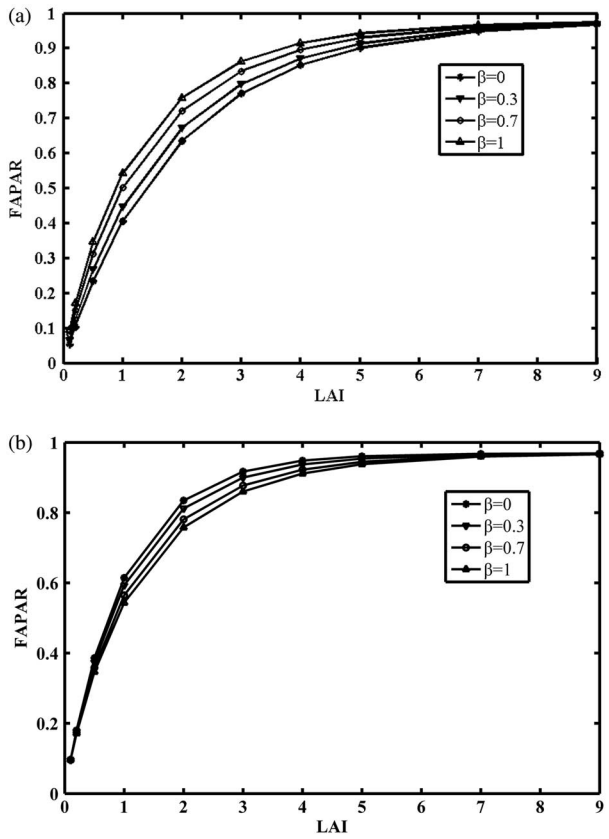

Fig. 11. Relationships between FAPAR and β from the model. (a) FAPAR ($\theta = 0°$). (b) FAPAR ($\theta = 60°$).

Fig. 12. Geographic position of the study area.

30 m, was used in this study. The latitude and longitude were $38°32'38''-39°28'19''$N and $99°51'54''-100°50'56''$E. Geometric correction, atmospheric correction, and radiometric calibration were performed before the data were used. The 6S model was selected for atmospheric correction, and the aerosol light depth was obtained by a sounding balloon. Spectral changes in vegetation and soil before and after atmospheric correction are shown in Fig. 14(a). The airborne hyperspectral data (CASI data) were obtained synchronously. The HJ-CCD and CASI spectra (atmospherically corrected by FLAASH) are shown in

Fig. 13. PAR measurement above the canopy.

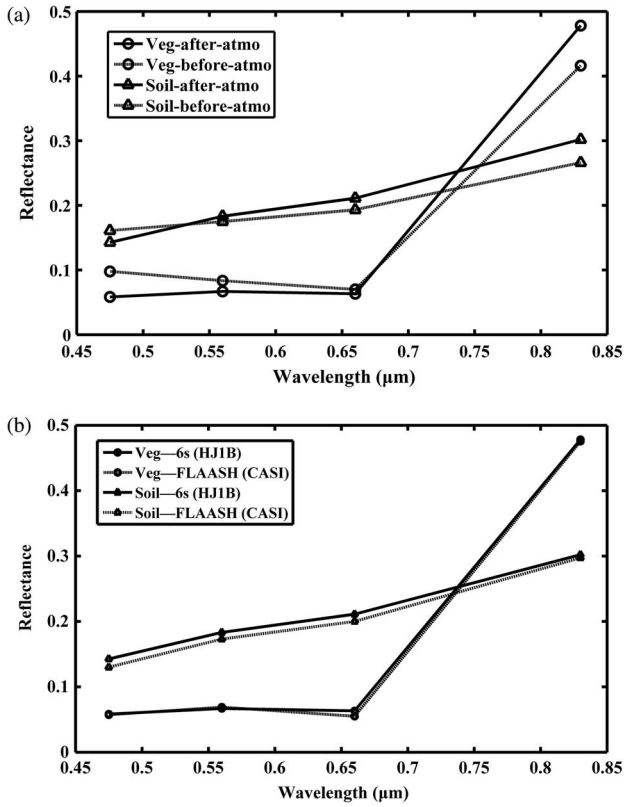

Fig. 14. Spectral changes in vegetation and soil: (a) before and after atmospheric correction and (b) after atmospheric correction using 6S model and FLAASH.

Fig. 14(b). We found that the accuracy of atmospheric correction is acceptable.

B. FAPAR Retrieval

A hybrid model of canopy reflectance [54], [55] was used to calculate LAI in this paper. A lookup table was built to facilitate LAI retrieval. The LAI retrieval results are shown in Fig. 15(a).

As indicated by (10) and (11), many input parameters are required for FAPAR retrieval. G was set to 0.5 (assuming that the leaf-angle distribution was spherical), and leaf reflectance, leaf transmittance, and soil reflectance were obtained by field measurement using an ASD spectrometer. Solar zenith angle (θ) was obtained from the image header file; the recollision probability (p) was calculated using an empirical formula; and the diffuse

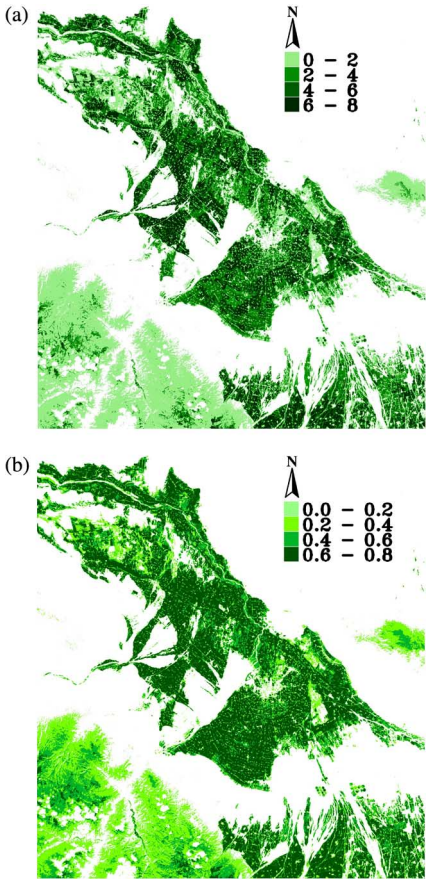

Fig. 15. LAI and FAPAR retrieval results: (a) LAI and (b) FAPAR.

skylight proportion (β) was obtained from SunScan BF3 observations as $\beta = 0.3$. FAPAR could be retrieved directly using the FAPAR-P model, with results shown in Fig. 15(b).

C. Field Validation

The algorithm was validated using daily FAPAR measurements for the corn canopy. To perform field validation, 75 simultaneous synchronous sets from 12 different quadrats were selected to validate the FAPAR.

The transit time of the HJ-1B image was 11:52, but the field data were collected from 13:00 to 17:00. Temporal normalization was performed according to the FAPAR diurnal variation observed on July 8, as shown in Fig. 16.

Fig. 17 shows the difference between the retrieved and measured FAPAR values. The error is small and acceptable (less than 5%), indicating the feasibility of the proposed model.

As the MODIS LAI/FPAR product is the most popular global product, and has been proved to be reliable [56], [57]. So the MODIS FAPAR product (MOD15) was used to compare with the model-calculated FAPAR values. Data from MOD15 (July 11, 2002) in the midstream area of the Heihe Basin were selected. MOD15 provides FAPAR products with 1-km resolution. First, the MOD15 LAI product was used as an input parameter; other input parameters were given as follows: G was set to 0.5, leaf reflectance and soil reflectance were obtained by field measurement using an ASD spectrometer. Solar zenith angle (θ) was obtained from the image header file; p was calculated using

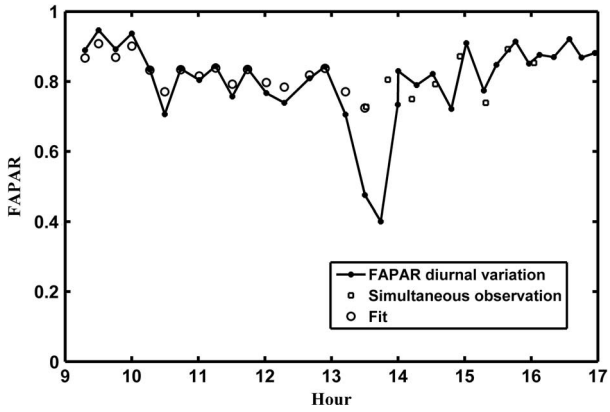

Fig. 16. APAR diurnal variation, simultaneous observations, and fitted values.

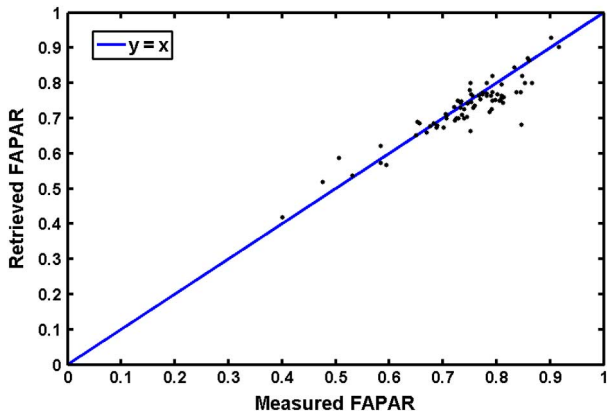

Fig. 17. Difference between retrieved and measured FAPAR.

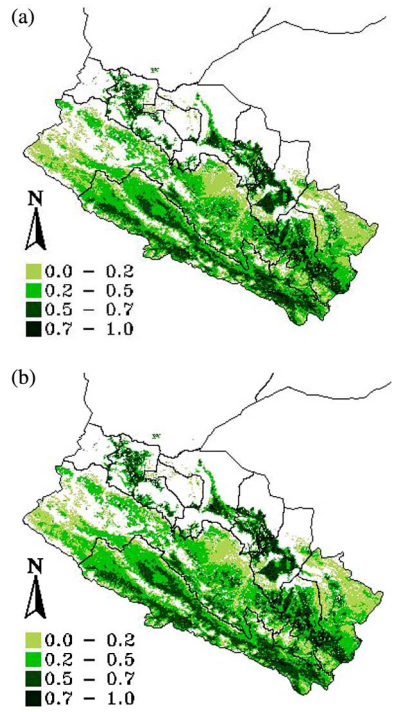

Fig. 18. Comparison of FAPAR retrieval result and FAPAR product: (a) FAPAR calculated by FAPAR-P and (b) MOD15 FPAR product.

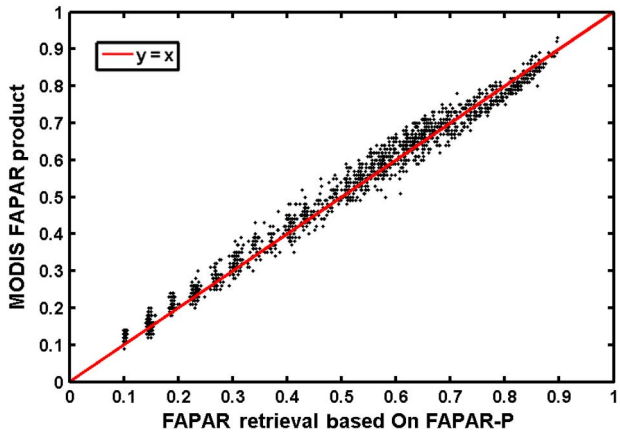

Fig. 19. Comparison of FAPAR retrieval result and FAPAR product.

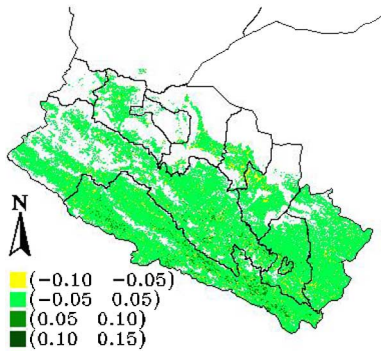

Fig. 20. Difference of FAPAR retrieval result and FAPAR product.

empirical formula; and β was obtained from SunScan BF3 observations. Then FAPAR was calculated in the FAPAR retrieval model. The FAPAR derived using FAPAR-P and MODIS FAPAR product were then compared, as shown in Figs. 18 and 19. The FAPAR retrieval result from FAPAR-P showed good consistency with the MOD15 product. The difference of two results was shown in Fig. 20. We found that there are also some small difference between the FAPAR retrieval result and FAPAR MOD15 product in forest and crop area. In coniferous forests of upstream, the result of FAPAR-P model is a little higher than MOD15 product. In crop area located in midstream, it is a little lower than MOD15 product, and more approach to the retrieval result of HJ-1B.

V. Conclusion and Discussion

In this research, a new quantitative model has been developed to improve FAPAR retrieval precision. The model considers multiple scattering both within the canopy and between the canopy and the soil, as well as diffuse sky radiation. The FAPAR-P model can also be extended to row crops and discrete vegetation canopies using effective LAI instead of LAI.

It has been proved that the new model is reliable and effective in acquiring canopy FAPAR by comparing the results of the model and of MC simulations. Then solar zenith angle, LAI, and other factors that affect the retrieval of canopy FAPAR were discussed in a preliminary way. Finally, ground validation of the model was conducted, and the results showed that the difference between the retrieved FAPAR and field measurements is small. However, the FAPAR-P model has not been verified in a forest canopy because the FAPAR of forest canopies is difficult to obtain. This will be the next step in this study.

The FAPAR retrieval algorithm separates diffuse radiation from direct solar radiation. Because diffuse skylight is separated, the model provides a new basis for FAPAR study under cloudy weather. This will be another future research direction on FAPAR retrieval.

References

[1] G. P. Asner, C. A. Wessman, and S. Archer, "Scale dependence of absorption of photosynthetically active radiation in terrestrial ecosystems," *Ecol. Appl.*, vol. 8, no. 4, pp. 1003–1021, Nov. 1998.

[2] A. Ruimy, P. G. Jarvis, D. D. Baldocchi, and B. Saugier, "CO2 fluxes over plant canopies and solar radiation: A review," *Adv. Ecol. Res.*, vol. 26, pp. 1–68, 1995.

[3] D. Baldocchi, "Measuring and modelling carbon dioxide and water vapour exchange over a temperate broad-leaved forest during the 1995 summer drought," *Plant Cell Environ.*, vol. 20, no. 9, pp. 1108–1122, Sep. 1997.

[4] E. Falge, D. Baldocchi, and R. Olson, "Gap-filling strategies for defensible annual sums of net ecosystem exchange," *Agric. Forest Meteorol.*, vol. 107, no. 1, pp. 43–69, Mar. 2001.

[5] S. Lafont *et al.*, "Spatial and temporal variability of land CO2 fluxes estimated with remote sensing and analysis data over western Eurasia," *Tellus B Chem. Phys. Meteorol.*, vol. 54, no. 5, pp. 820–833, Nov. 2002.

[6] P. Mahadevan *et al.*, "A satellite-based biosphere parameterization for net ecosystem CO2 exchange: Vegetation photosynthesis and respiration model (VPRM)," *Global Biogeochem. Cycles*, vol. 22, no. 2, pp. 1–17, 2008.

[7] D. P. Turner *et al.*, "Assessing FPAR source and parameter optimization scheme in application of a diagnostic carbon flux model," *Remote Sens. Environ.*, vol. 113, no. 7, pp. 1529–1539, Jul. 2009.

[8] S. D. Prince and S. N. Goward, "Global primary production: A remote sensing approach," *J. Biogeogr.*, vol. 22, no. 4/5, pp. 815–835, Jul./Sep. 1995.

[9] A. Ruimy, L. Kergoat, and A. Bondeau, "Comparing global models of terrestrial net primary productivity (NPP): Analysis of differences in light absorption and light-use efficiency," *Global Change Biol.*, vol. 5, pp. 56–64, Apr. 1999.

[10] R. B. Myneni *et al.*, "Global products of vegetation leaf area and fraction absorbed PAR from year one of MODIS data," *Remote Sens. Environ.*, vol. 83, no. 1–2, pp. 214–231, Nov. 2002.

[11] J. T. Morisette *et al.*, "Validation of global moderate-resolution LAI products: A framework proposed within the CEOS land product validation subgroup," *IEEE Trans. Geosci. Remote Sens.*, vol. 44, no. 7, pp. 1804–1817, Jul. 2006.

[12] N. Gobron *et al.*, "Evaluation of fraction of absorbed photosynthetically active radiation products for different canopy radiation transfer regimes: Methodology and results using joint research center products derived from SeaWiFS against ground-based estimations," *J. Geophys. Res.*, vol. 111, no. D13, pp. 1–15, Jul. 2006.

[13] D. D. Baldocchi and P. C. Harley, "Scaling carbon dioxide and water vapour exchange from leaf to canopy in a deciduous forest, II. Model testing and application," *Plant Cell Environ.*, vol. 18, no. 10, pp. 1157–1173, Oct. 1995.

[14] P. De Reffye, C. Edelin, J. Françon, and M. Jaeger, "Plant models faithful to botanical structure and development," in *Proc. ACM SIGGRAPH*, Aug. 1988, vol. 22, pp. 151–158.

[15] H. Sinoquet *et al.*, "RATP: A model for simulating the spatial distribution of radiation absorption, transpiration and photosynthesis within canopies: Application to an isolated tree crown," *Plant Cell Environ.*, vol. 24, no. 4, pp. 395–406, Apr. 2001.

[16] J. Dauzat, B. Rapidel, and A. Berger, "Simulation of leaf transpiration and sap flow in virtual plants: Model description and application to a coffee plantation in Costa Rica," *Agric. Forest Meteorol.*, vol. 109, no. 2, pp. 143–160, Aug. 2001.

[17] P. J. Sellers, J. A. Berry, G. J. Collatz, C. B. Field, and F. G. Hall, "Canopy reflectance, photosynthesis, and transpiration, III. A reanalysis using improved leaf models and a new canopy integration scheme," *Remote Sens. Environ.*, vol. 42, no. 3, pp. 187–216, Dec. 1992.

[18] J. S. Amthor, M. L. Goulden, J. W. Munger, and S. C. Wofsy, "Testing a mechanistic model of forest-canopy mass and energy exchange using eddy correlation: Carbon dioxide and ozone uptake by a mixed oak-maple stand," *Aust. J. Plant Physiol.*, vol. 21, no. 5, pp. 623–651, 1994.
[19] J. Lloyd *et al.*, "A simple calibrated model of Amazon rainforest productivity based on leaf biochemical properties," *Plant Cell Environ.*, vol. 18, no. 10, pp. 1129–1145, Oct. 1995.
[20] T. R. Sinclair, C. E. Murphy, and K. R. Knoerr, "Development and evaluation of simplified models for simulating canopy photosynthesis and transpiration," *J. Appl. Ecol.*, vol. 13, no. 3, pp. 813–829, Dec. 1976.
[21] J. M. Norman, "Interfacing leaf and canopy irradiance interception models," *Plant Photosynth.*, vol. 2, pp. 49–67, 1980.
[22] D. G. G. Pury and G. D. Farquhar, "Simple scaling of photosynthesis from leaves to canopies without the errors of big-leaf models," *Plant Cell Environ.*, vol. 20, pp. 537–557, May 1997.
[23] Y. P. Wang and R. Leuning, "A two-leaf model for canopy conductance, photosynthesis and partitioning of available energy, I: Model description and comparison with a multi-layered model," *Agric. Forest Meteorol.*, vol. 91, no. 1–2, pp. 89–111, May 1998.
[24] R. Leuning, F. X. Dunin, and Y. P. Wang, "A two-leaf model for canopy conductance, photosynthesis and partitioning of available energy, II: Comparison with measurements," *Agric. Forest Meteorol.*, vol. 91, no. 1–2, pp. 113–125, May 1998.
[25] R. E. Dickinson, "Biosphere/atmosphere transfer scheme (BATS) for the NCAR community climate model," NCAR Tech. Note, TN-275 +STR, p. 69, 1986.
[26] P. J. Sellers and Y. Mintz, "A simple biosphere model (SIB) for use within general circulation models," *Clim. J.*, vol. 43, no. 6, pp. 505–531, Mar. 1986.
[27] P. J. Sellers *et al.*, "A revised land surface parameterization (SiB2) for atmospheric GCMS: Part I: Model formulation," *Clim. J.*, vol. 9, no. 4, pp. 676–705, Apr. 1996.
[28] E. A. Kowalczyk, J. R. Garratt, and P. B. Krummel, "A soil-canopy scheme for use in a numerical model of the atmosphere: 1D stand-alone model," *CSIRO Div. Atmos. Res.*, Tech. Paper, vol. 23, p. 56, 1991.
[29] E. A. Kowalczyk, J. R. Garratt, and P. B. Krummel, "Implementation of a soil-canopy scheme into the CSIRO GCM: Regional aspects of the model response," *CSIRO Div. Atmos. Res.*, Tech. Paper, vol. 32, p. 59, 1994.
[30] J. R. Garratt, "Sensitivity of climate simulations to land-surface and atmospheric boundary-layer treatments—a review," *Clim. J.*, vol. 6, no. 3, pp. 419–448, Mar. 1993.
[31] Q. Y. Zhang, E. M. Middleton, Y. B. Cheng, and D. R. Landis, "Variations of foliage chlorophyll fAPAR and foliage non-chlorophyll fAPAR (fAPARchl, fAPARnonchl) at the Harvard Forest," *IEEE J. Sel. Topics Appl. Earth Observ. Remote Sens.*, vol. 6, no. 5, pp. 2254–2264, Oct. 2013.
[32] S. W. Running, D. D. Baldocchi, and D. P. Turner, "A global terrestrial monitoring network integrating tower fluxes, flask sampling, ecosystem modeling, and EOS satellite data," *Remote Sens. Environ.*, vol. 70, no. 1, pp. 108–127, Oct. 1999.
[33] D. P. Turner, S. V. Ollinger, and J. S. Kimball, "Integrating remote sensing and ecosystem process models for landscape-to regional-scale analysis of the carbon cycle," *BioScience*, vol. 54, no. 6, pp. 573–584, 2004.
[34] N. Gobron, B. Pinty, O. Aussedat, and M. Taberner, "Uncertainty estimates for the FAPAR operational products derived from MERIS—Impact of top-of-atmosphere radiance uncertainties and validation with field data," *Remote Sens. Environ.*, vol. 112, no. 4, pp. 1871–1883, Apr. 2008.
[35] R. Fensholt, I. Sandholt, and M. S. Rasmussen, "Evaluation of MODIS LAI, fAPAR and the relation between fAPAR and NDVI in a semi-arid environment using in-situ measurements," *Remote Sens. Environ.*, vol. 91, pp. 490–507, Jun. 2004.
[36] Y. Knyazikhin *et al.*, "Synergistic algorithm for estimating vegetation canopy leaf area index and fraction of absorbed photosynthetically active radiation from MODIS and MISR data," *J. Geophys. Res.*, vol. 103, pp. 32257–32276, Dec. 1998.
[37] F. Deng, J. M. Chen, and S. Plummer, "Algorithm for global leaf area index retrieval using satellite imagery," *IEEE Trans. Geosci. Remote Sens.*, vol. 44, no. 8, pp. 2219–2229, Aug. 2006.
[38] F. Baret, O. Hagolle, B. Geiger, and P. Bicheron, "LAI, fAPAR, and fCover CYCLOPES global products derived from vegetation: Part 1: Principles of the algorithm," *Remote Sens. Environ.*, vol. 110, no. 3, pp. 275–286, Oct. 2007.
[39] N. Gobron, B. Pinty, M. M. Verstraete, and Y. Govaerts, "The MERIS global vegetation index (MGVI): Description and preliminary application," *Int. J. Remote Sens.*, vol. 20, no. 9, pp. 1917–1927, 1999.
[40] N. Gobron *et al.*, "A global vegetation index for SeaWiFS: Design and applications," *Remote Sens. Clim. Model. Synergies Limit.*, vol. 7, pp. 5–21, 2001.
[41] N. Gobron *et al.*, "Evaluation of the MERIS/ENVISAT fAPAR product," *Adv. Space Res.*, vol. 39, no. 1, pp. 105–115, 2007.
[42] N. Gobron, B. Pinty, M. M. Verstraete, and Y. Govaerts, "A semidiscrete model for the scattering of light by vegetation," *J. Geophys. Res. Atmos.*, vol. 102, no. D8, pp. 9431–9446, Apr. 1997.
[43] T. Manninen and P. Stenberg, "Simulation of the effect of snow-covered forest floor on the total forest albedo," *Agric. Forest Meteorol.*, vol. 149, pp. 303–319, Feb. 2009.
[44] T. Nilson, "A theoretical analysis of the frequency gaps in plant stands," *Agric. Forest Meteorol.*, vol. 8, pp. 25–28, 1971.
[45] J. M. Chen, "Optically based methods for measuring seasonal variation of leaf area index in boreal conifer stands," *Agric. Forest Meteorol.*, vol. 80, no. 1–2, pp. 135–163, Jul. 1996.
[46] J. M. Chen, P. M. Rich, S. T. Gower, J. M. Norman, and S. Plummer, "Leaf area index of boreal forests: Theory, techniques, and measurements," *J. Geophys. Res. Atmos.*, vol. 102, no. D24, pp. 29429–29443, Dec. 1997b.
[47] M. Disney, P. Lewis, T. Quaife, and C. Nichol, "A spectral invariant approach to modeling canopy and leaf scattering," in *Proc. 9th Int. Symp. Phys. Meas. Signatures Remote Sens. (ISPMSRS)*, 2005, pp. 318–320.
[48] N. Metropolis and S. Ulam, "The Monte Carlo method," *J. Amer. Stat. Assoc.*, vol. 44, pp. 335–341, 1949.
[49] Y. A. Shreider *et al.*, *The Monte Carlo Method: The Method of Statistical Trials*. New York, NY, USA: Pergamon, 1966.
[50] Y. M. Govaerts and M. M. Verstraete, "Raytran: A Monte Carlo ray-tracing model to compute light scattering in three-dimensional heterogeneous media," *IEEE Trans. Geosci. Remote Sens.*, vol. 36, no. 2, pp. 493–505, Mar. 1998.
[51] S. L. Liang, X. W. Li, and J. D. Wang, "Advanced remote sensing," *Terr. Inf. Extract. Appl.*, pp. 386–388, 2013.
[52] S. Smolander and P. Stenberg, "Simple parameterizations of the radiation budget of uniform broadleaved and coniferous canopies," *Remote Sens. Environ.*, vol. 94, pp. 355–363, Feb. 2005.
[53] B. Y. Yan, X. R. Xu, and W. J. Fan, "A unified canopy bidirectional reflectance (BRDF) model for row crops," *Sci. China Earth*, vol. 42, no. 3, pp. 411–423, 2012.
[54] H. R. Jin *et al.*, "Monitoring the spatial distribution of leaf area index in high-resolution pixels based on BJ-1 data," *Prog. Nat. Sci.*, vol. 17, pp. 1229–1234, Jul. 2007, in Chinese.
[55] W. J. Fan, X. R. Xu, X. C. Liu, B. Y. Yan, and Y. K. Cui, "Accurate LAI retrieval method based on PROBA/CHRIS data," *Hydrol. Earth Syst. Sci.*, vol. 14, pp. 1–9, 2010.
[56] Y. H. Tian, "Evaluation of the performance of the MODIS LAI and FPAR algorithm with multi-resolution satellite data," Ph.D. dissertation, Boston Univ., Boston, MA, USA, 2002.
[57] S. P. Serbin, D. E. Ahl, and S. T. Gower, "Spatial and temporal validation of the MODIS LAI and FPAR products across a boreal forest wildfire chronosequence," *Remote Sens. Environ.*, vol. 133, pp. 71–84, Jun. 2013.

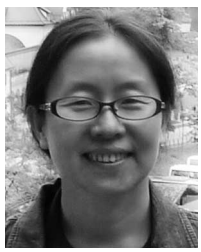

Wenjie Fan received the Ph.D. degree in physical geography from the Department of Urban and Environmental Sciences, Peking University (PKU), Beijing, China, in 2000, and completed the Postdoctorate Research from the Institute of Remote Sensing and GIS (IRSGIS), PKU, in 2002.

She is an Associate Professor with the IRSGIS, PKU. She has continued to work on and manage research projects on vegetation remote sensing, scale effects of remote sensing, hyperspectral remote sensing, and application of remote sensing in ecology and environment management for 11 years.

Yuan Liu received the Master of Engineering degree from the Peking University, Beijing, China, in 2013.

Her research interests include FAPAR retrieval, LAI retrieval of vegetation, and other quantitative remote-sensing models.

Xiru Xu (M) received the Bachelor of Science degree from the Department of Geophysics, Peking University (PKU), Beijing, China, in 1960.

He is a Professor of Institute of Remote Sensing and GIS (IRSGIS), PKU. From 1981 to 1983, he was a Visiting Scholar of Electrical Engineering and Computer Science Department, MIT, Cambridge, MA, USA. He has continued to work on and manage research projects on quantitative remote sensing, microwave remote sensing, and vegetation remote sensing for more than 30 years.

Gaoxing Chen received the B.Sc. degree from Wuhan University, Wuhan, China, in 2011, and is pursuing the Master's degree at the Peking University.

His research interests include vegetation remote sensing, especially about recollision probability, and vegetation canopy BRDF model.

Beitong Zhang received the B.S. degree in geographical information system from Peking University, Beijing, China in 2013, and is pursuing the Master's degree in remote sensing at the Peking University.

His research interests include vegetation remote sensing, especially about vegetation canopy's Monte Carlo model.